class of deacetylase activity. Sirtinol counteracted the CBF retention at 2 hours after BCAS (vehicle group, 87.1±3.6% versus sirtinol group, 66.8±3.3%; Figure 4B). It is notable that CBF of sirtinol-treated Sirt1-Tg mice was lower than that of wild-type littermates (74.3±3.2%), indicating that sirtinol inhibited the endogenous SIRT1 (plus other sirtuins expressed in cerebral blood vessels). Sham operation did not alter CBF of sirtinol-treated Sirt1-Tg mice (Figure IV in the online-only Data Supplement). Thus, the deacetylating activity of SIRT1 is required for the maintenance of CBF after cerebral hypoperfusion in Sirt1-Tg and wild-type mice.

Sirt1-Tg Mice Exhibit a Higher Cerebral Vasodilatory Response to an eNOS Agonist

A previous in vitro study suggested that the vasodilating activity of eNOS is potentiated by SIRT1.[26] To test the possible involvement of eNOS in the phenotype of Sirt1-Tg mouse, we measured CBF before and after the exposure with a classical eNOS agonist acetylcholine. CBF of Sirt1-Tg mice showed significantly larger response to acetylcholine than that of wild-type littermates (Sirt1-Tg, 18.8±3.3% versus wild-type, 8.0±1.8%; Figure 5A and 5C). In vivo vessel imaging with fluorescein isothiocyanate-dextran corroborated the results with vasodilatory responses to acetylcholine (Sirt1-Tg, 7.01±0.83% versus wild-type, 3.65±0.44%; Figure 5B and 5D). We also used S-Nitroso-N-acetyl-DL-penicillamine, a nitric oxide (NO) donor, instead of acetylcholine, and determined whether the whole NOS machinery can be bypassed to raise CBF in both genotypes. Wild-type and Sirt1-Tg mice showed similar increase in CBF in response to S-Nitroso-N-acetyl-DL-penicillamine, which was relatively greater than the response to acetylcholine (Figure V in the online-only Data Supplement).

Excess SIRT1 Suppresses eNOS Acetylation After BCAS

To explore the molecular pathway involved in our in vivo findings, we conducted biochemical analyses. The levels of the total eNOS in the brain homogenates did not differ between wild-type and Sirt1-Tg littermates, both before and at 2 hours after BCAS. The cerebral protein level of Ser1177-phosphorylated eNOS increased at 2 hours after BCAS in wild-type mice, but not in Sirt1-Tg mice, reflecting lack of vascular endothelial growth factor–mediated compensatory response after CBF reduction[27] in Sirt1-Tg mice. To detect deacetylated eNOS specifically, brain homogenates before

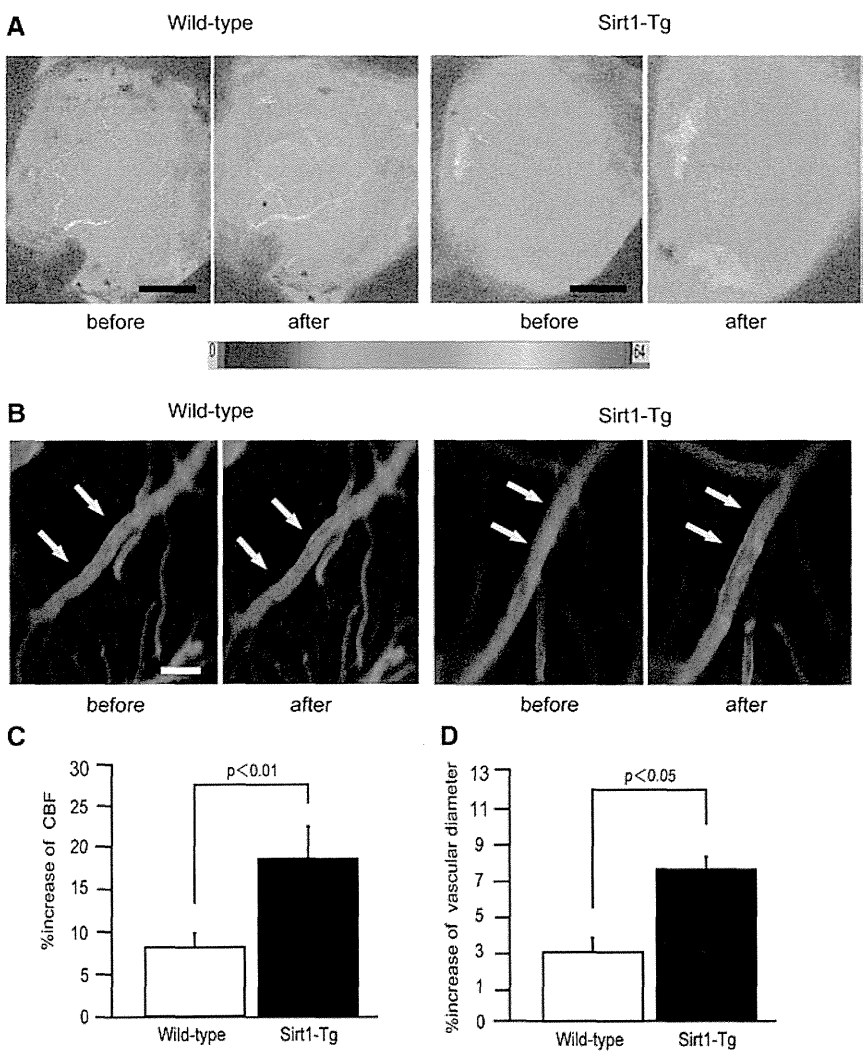

Figure 5. *Sirt1*-overexpressing (Sirt1-Tg) mice exhibited increased vasodilative response to acetylcholine (ACh). Temporal changes in cerebral blood flow (CBF) assessed by laser speckle flowmetry (**A**) and in diamteters of leptomeningeal arteries (**B**) before (**left**) and after (**right**) perfusion of ACh on brain surface in wild-type and Sirt1-Tg mice. Scale bars indicate 1 mm (**A**) and 50 μm (**B**). Histograms showing % increase of CBF assessed by laser speckle flowmetry (**C**) and % increase of vascular diameter (**D**) in response to ACh in wild-type (n=6) and Sirt1-Tg mice (n=6).

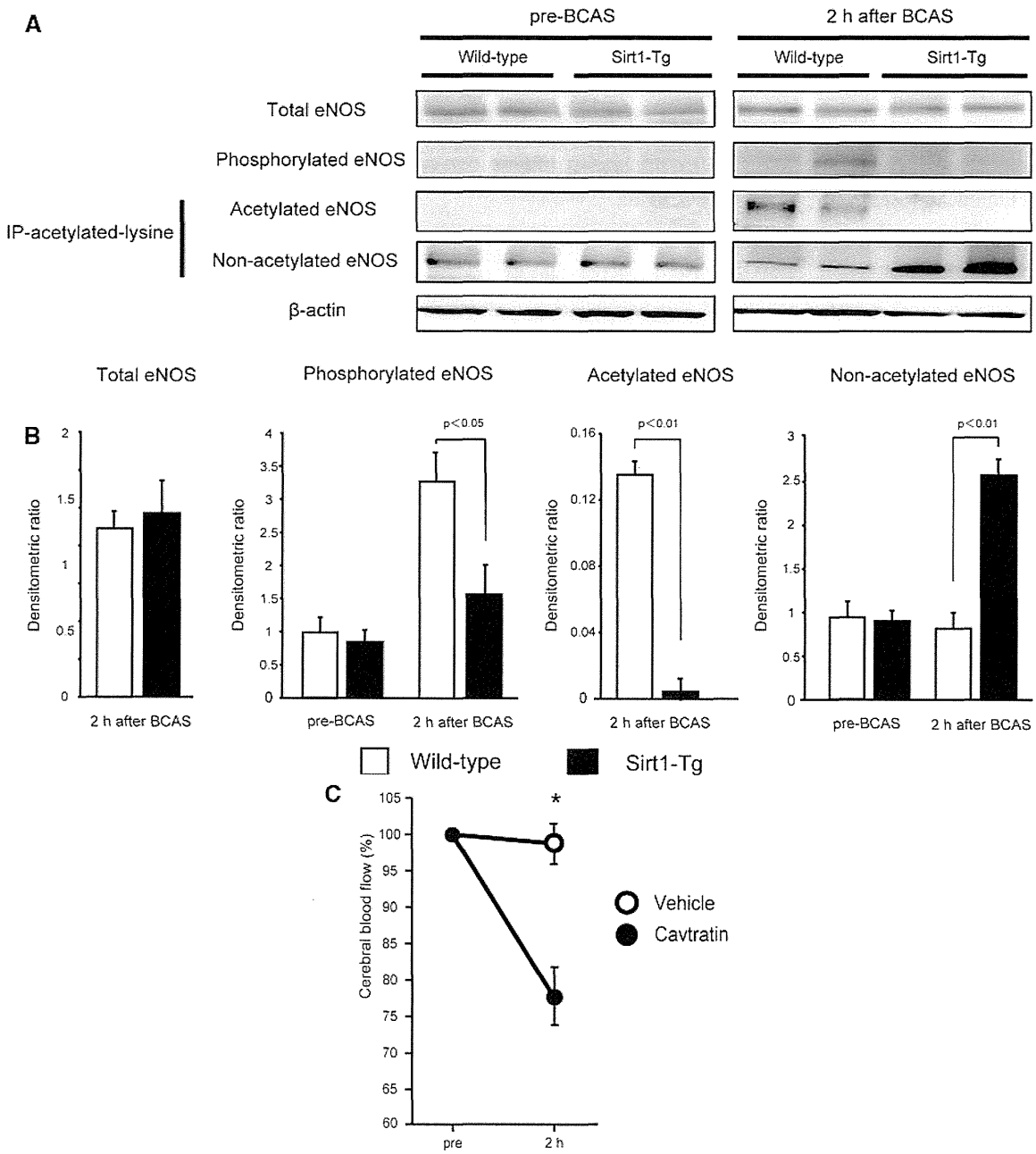

Figure 6. Endothelial nitric oxide synthase (eNOS) was completely deacetylated in *Sirt1*-overexpressing (Sirt1-Tg) mice at 2 hours after bilateral common carotid artery stenosis (BCAS). **A**, Immunoblots of total eNOS, phosphorylated eNOS, acetylated eNOS, and nonacetylated eNOS and β-actin of wild-type and Sirt1-Tg mice before and at 2 hours after BCAS. The results of 2 different animals for each genotype are shown. Similar results were obtained in 2 other animals. **B**, Histogram showing the ratio of eNOS, phosphorylated eNOS, acetylated eNOS, and nonacetylated eNOS to β-actin. **C**, Cerebral blood flow of vehicle-treated Sirt1-Tg mice (n=7) and cavtratin-treated Sirt1-Tg mice (n=6) before and at 2 hours after BCAS. **P*<0.01 vs vehicle.

and at 2 hours after operation were immunoprecipitated with antibodies against acetylated lysine, and the immunoprecipitates were probed with antibodies against eNOS to detect acetylated eNOS. Intriguingly, acetylated eNOS was undetectable in the both groups before BCAS, whereas it became detectable only in wild-type mice after BCAS. In the pooled elution fractions that are expected to contain nonacetylated eNOS, brain tissues from Sirt1-Tg mice contained greater amounts of nonacetylated eNOS compared with those from wild-type littermates after BCAS, but the amounts of nonacetylated eNOS before BCAS in both groups were similar (Figure 6A and 6B).

CBF Retention in Sirt1-Tg Mice After BCAS Is Abolished by eNOS Inactivation

To verify the requirement of eNOS activation for the CBF retention in Sirt1-Tg mice after BCAS, we treated them with an eNOS inhibitor, cavtratin (caveolin-1 scaffolding domain peptide, 10 mg/kg per day 3× days). Cavtratin significantly reduced CBF of Sirt1-Tg mice at 2 hours after

BCAS (cavtratin, 77.7±4.1% versus vehicle, 97.3±3.9%; each normalized with the baseline CBF; Figure 6C), offsetting the increment of CBF by the overexpression of SIRT1 (cf. Figures 4A and 6C). Sham operation did not alter CBF of cavtratin-treated Sirt1-Tg mice (Figure VI in the online-only Data Supplement). These results suggest that the SIRT1-mediated deacetylation activates eNOS, which counters the perfusion failure after BCAS.

Discussion

Using Sirt1-overexpressing Tg mice, we found that endothelial SIRT1 deacetylates and activates eNOS and thus normalizes CBF after BCAS. These effects were abolished by treatment with inhibitors of SIRT1 or eNOS in Sirt1-Tg mice, suggesting that SIRT1–eNOS–NO system is responsible for the CBF-preserving effect after cerebral hypoperfusion. SIRT1 overexpression also significantly attenuated BCAS-induced blood–brain barrier disruption, glial activation, myelin loss, and working memory impairment. Furthermore, SIRT1 overexpression suppressed alterations in the vascular microarchitecture and any neuronal derangement. These results firstly show that SIRT1 has a robust role in suppressing the consequence of cerebral hypoperfusion by activating a cerebral NO-dependent mechanism.

Our results are congruent with a previous in vitro study showing that SIRT1 and eNOS colocalize and coprecipitate in endothelial cells and that SIRT1 can deacetylate eNOS.[26] Therefore, an interaction of SIRT1 with eNOS may mediate cerebrovascular protection by facilitating NO-dependent vascular relaxation, which has been firstly demonstrated in vivo in the current study. Oxidative stress is known to trigger acetylation of eNOS in endothelial cells, leading to inactivation of eNOS activity.[28] Based on the current finding that the fall in CBF after BCAS is prevented in Sirt1-Tg mice and our previous finding that the gradual CBF recovery after BCAS was markedly inhibited with NOS inhibitor N^{ω}-nitro-L-arginine methyl ester,[29] cerebral SIRT1–eNOS–NO system may regulate physiological energy stability in the brain.

Accumulating evidence suggests that SIRT1 plays an important role in neurodegenerative diseases through different pathways.[8–11] Alzheimer disease is one of neurodegenerative diseases, but vascular pathology contributes to Alzheimer disease changes to variable degrees.[30–34] There is an emerging concept of protein elimination failure arteriopathy[35] where waste products such as amyloid-β accumulate in the brain as a result of cerebral perfusion failure and evoke disparate brain disorders because perivascular drainage of waste products are driven by arterial pulsation.[36] Because reduced amyloid-β clearance from the brain seems to be mainly responsible for the pathogenesis of sporadic Alzheimer disease,[37] the drainage of extracellular amyloid-β along the arteries seems to be a significant strategy for removal of amyloid-β from the brain.[33,38–40] The CBF-preserving effect of SIRT1 may provide a unified scheme for treatment of broad spectrum of brain diseases involving both cerebrovascular and neurodegenerative mechanisms.

In conclusion, our study provides strong evidence for the role of SIRT1 in protection of the brain after cerebral hypoperfusion and ischemic injury by activating the eNOS–NO system. The robust effects of SIRT1 overexpression on restoration of cerebrovascular reserve in mice may explain the positive effects of SIRT1 reported in animal models of ischemic injury and neurodegeneration. However, it remains to be determined whether sirtuin-activating compounds such as resveratrol can be used as proof of concept agents for novel strategies for the treatment of disparate brain disorders.

Acknowledgments

We acknowledge the gift of the mouse *Sirt1* cDNA and the thoughtful comments from Dr Shin-ichiro Imai and thank Dr Ahmad Khundakar for editing the article. We are indebted to Takako Kawada for her excellent technical assistance in staining and tissue sections.

Sources of Funding

We gratefully acknowledge grant support from the Ministry of Health, Labour, and Welfare (Dr Ihara, no. 0605-1), the Ministry of Education, Culture, Sports, Science, and Technology (Dr Ihara, Grant-in-Aid for Scientific Research (B), no. 23390233; Dr Hattori, Grant-in-Aid for Research Activity Start-up, no. 25893301; Dr Kinoshita, Grant-in-Aid for Scientific Research on Innovative Areas, no. 2311531 and 25116514), the Takeda Science Foundation (Dr Ihara), Japan Science Technology Corporation (Dr Takahashi), and Alzheimer's Research UK (Dr Kalaria).

Disclosures

None.

References

1. Klar AJ, Fogel S, Macleod K. MAR1-a regulator of the HMa and HMalpha loci in Saccharomyces cerevisiae. *Genetics*. 1979;93:37–50.
2. Duan W. Sirtuins: from metabolic regulation to brain aging. *Front Aging Neurosci*. 2013;5:36.
3. Imai S, Armstrong CM, Kaeberlein M, Guarente L. Transcriptional silencing and longevity protein Sir2 is an NAD-dependent histone deacetylase. *Nature*. 2000;403:795–800.
4. Howitz KT, Bitterman KJ, Cohen HY, Lamming DW, Lavu S, Wood JG, et al. Small molecule activators of sirtuins extend Saccharomyces cerevisiae lifespan. *Nature*. 2003;425:191–196.
5. Tissenbaum HA, Guarente L. Increased dosage of a sir-2 gene extends lifespan in Caenorhabditis elegans. *Nature*. 2001;410:227–230.
6. Rogina B, Helfand SL. Sir2 mediates longevity in the fly through a pathway related to calorie restriction. *Proc Natl Acad Sci U S A*. 2004;101:15998–16003.
7. Satoh A, Brace CS, Rensing N, Cliften P, Wozniak DF, Herzog ED, et al. Sirt1 extends life span and delays aging in mice through the regulation of Nk2 homeobox 1 in the DMH and LH. *Cell Metab*. 2013;18:416–430.
8. Donmez G, Wang D, Cohen DE, Guarente L. SIRT1 suppresses beta-amyloid production by activating the alpha-secretase gene ADAM10. *Cell*. 2010;142:320–332.
9. Min SW, Cho SH, Zhou Y, Schroeder S, Haroutunian V, Seeley WW, et al. Acetylation of tau inhibits its degradation and contributes to tauopathy. *Neuron*. 2010;67:953–966.
10. Yeung F, Hoberg JE, Ramsey CS, Keller MD, Jones DR, Frye RA, et al. Modulation of NF-kappaB-dependent transcription and cell survival by the SIRT1 deacetylase. *EMBO J*. 2004;23:2369–2380.
11. Wang R, Li JJ, Diao S, Kwak YD, Liu L, Zhi L, et al. Metabolic stress modulates Alzheimer's β-secretase gene transcription via SIRT1-PPARγ-PGC-1 in neurons. *Cell Metab*. 2013;17:685–694.
12. Wareski P, Vaarmann A, Choubey V, Safiulina D, Liiv J, Kuum M, et al. PGC-1{alpha} and PGC-1{beta} regulate mitochondrial density in neurons. *J Biol Chem*. 2009;284:21379–21385.
13. Kim D, Nguyen MD, Dobbin MM, Fischer A, Sananbenesi F, Rodgers JT, et al. SIRT1 deacetylase protects against neurodegeneration in models for Alzheimer's disease and amyotrophic lateral sclerosis. *EMBO J*. 2007;26:3169–3179.
14. Zhang F, Wang S, Gan L, Vosler PS, Gao Y, Zigmond MJ, et al. Protective effects and mechanisms of sirtuins in the nervous system. *Prog Neurobiol*. 2011;95:373–395.

15. Della-Morte D, Dave KR, DeFazio RA, Bao YC, Raval AP, Perez-Pinzon MA. Resveratrol pretreatment protects rat brain from cerebral ischemic damage via a sirtuin 1-uncoupling protein 2 pathway. *Neuroscience*. 2009;159:993–1002.
16. Hernández-Jiménez M, Hurtado O, Cuartero MI, Ballesteros I, Moraga A, Pradillo JM, et al. Silent information regulator 1 protects the brain against cerebral ischemic damage. *Stroke*. 2013;44:2333–2337.
17. Toledo JB, Arnold SE, Raible K, Brettschneider J, Xie SX, Grossman M, et al. Contribution of cerebrovascular disease in autopsy confirmed neurodegenerative disease cases in the National Alzheimer's Coordinating Centre. *Brain*. 2013;136(pt 9):2697–2706.
18. Kalaria RN, Ihara M. Dementia: vascular and neurodegenerative pathways-will they meet? *Nat Rev Neurol*. 2013;9:487–488.
19. Shibata M, Ohtani R, Ihara M, Tomimoto H. White matter lesions and glial activation in a novel mouse model of chronic cerebral hypoperfusion. *Stroke*. 2004;35:2598–2603.
20. Shibata M, Yamasaki N, Miyakawa T, Kalaria RN, Fujita Y, Ohtani R, et al. Selective impairment of working memory in a mouse model of chronic cerebral hypoperfusion. *Stroke*. 2007;38:2826–2832.
21. Watanabe S, Ageta-Ishihara N, Nagatsu S, Takao K, Komine O, Endo F, et al. SIRT1 overexpression ameliorates a mouse model of SOD1-linked amyotrophic lateral sclerosis via HSF1/HSP70 chaperone system. *Mol Brain*. 2014;7:62.
22. Dvir-Ginzberg M, Gagarina V, Lee EJ, Booth R, Gabay O, Hall DJ. Tumor necrosis factor α-mediated cleavage and inactivation of SirT1 in human osteoarthritic chondrocytes. *Arthritis Rheum*. 2011;63:2363–2373.
23. Simák J, Holada K, D'Agnillo F, Janota J, Vostal JG. Cellular prion protein is expressed on endothelial cells and is released during apoptosis on membrane microparticles found in human plasma. *Transfusion*. 2002;42:334–342.
24. Starke R, Drummond O, MacGregor I, Biggerstaff J, Gale R, Camilleri R, et al. The expression of prion protein by endothelial cells: a source of the plasma form of prion protein? *Br J Haematol*. 2002;119:863–873.
25. Pflanzner T, Petsch B, André-Dohmen B, Müller-Schiffmann A, Tschickardt S, Weggen S, et al. Cellular prion protein participates in amyloid-β transcytosis across the blood-brain barrier. *J Cereb Blood Flow Metab*. 2012;32:628–632.
26. Mattagajasingh I, Kim CS, Naqvi A, Yamamori T, Hoffman TA, Jung SB, et al. SIRT1 promotes endothelium-dependent vascular relaxation by activating endothelial nitric oxide synthase. *Proc Natl Acad Sci U S A*. 2007;104:14855–14860.
27. Osuka K, Watanabe Y, Usuda N, Nakazawa A, Tokuda M, Yoshida J. Modification of endothelial NO synthase through protein phosphorylation after forebrain cerebral ischemia/reperfusion. *Stroke*. 2004;35:2582–2586.
28. Arunachalam G, Yao H, Sundar IK, Caito S, Rahman I. SIRT1 regulates oxidant- and cigarette smoke-induced eNOS acetylation in endothelial cells: role of resveratrol. *Biochem Biophys Res Commun*. 2010;393:66–72.
29. Fujita Y, Ihara M, Ushiki T, Hirai H, Kizaka-Kondoh S, Hiraoka M, et al. Early protective effect of bone marrow mononuclear cells against ischemic white matter damage through augmentation of cerebral blood flow. *Stroke*. 2010;41:2938–2943.
30. de la Torre JC. Alzheimer disease as a vascular disorder: nosological evidence. *Stroke*. 2002;33:1152–1162.
31. Kalaria RN, Ballard C. Overlap between pathology of Alzheimer disease and vascular dementia. *Alzheimer Dis Assoc Disord*. 1999;13(suppl 3):S115–S123.
32. Kalaria RN. Vascular basis for brain degeneration: faltering controls and risk factors for dementia. *Nutr Rev*. 2010;68(suppl 2):S74–S87.
33. Kalaria RN, Akinyemi R, Ihara M. Does vascular pathology contribute to Alzheimer changes? *J Neurol Sci*. 2012;322:141–147.
34. Snowdon DA, Greiner LH, Mortimer JA, Riley KP, Greiner PA, Markesbery WR. Brain infarction and the clinical expression of Alzheimer disease. The Nun Study. *JAMA*. 1997;277:813–817.
35. Carare RO, Hawkes CA, Jeffrey M, Kalaria RN, Weller RO. Review: cerebral amyloid angiopathy, prion angiopathy, CADASIL and the spectrum of protein elimination failure angiopathies (PEFA) in neurodegenerative disease with a focus on therapy. *Neuropathol Appl Neurobiol*. 2013;39:593–611.
36. Arbel-Ornath M, Hudry E, Eikermann-Haerter K, Hou S, Gregory JL, Zhao L, et al. Interstitial fluid drainage is impaired in ischemic stroke and Alzheimer's disease mouse models. *Acta Neuropathol*. 2013;126:353–364.
37. Mawuenyega KG, Sigurdson W, Ovod V, Munsell L, Kasten T, Morris JC, et al. Decreased clearance of CNS beta-amyloid in Alzheimer's disease. *Science*. 2010;330:1774.
38. Hawkes CA, Härtig W, Kacza J, Schliebs R, Weller RO, Nicoll JA, et al. Perivascular drainage of solutes is impaired in the ageing mouse brain and in the presence of cerebral amyloid angiopathy. *Acta Neuropathol*. 2011;121:431–443.
39. Hawkes CA, Sullivan PM, Hands S, Weller RO, Nicoll JA, Carare RO. Disruption of arterial perivascular drainage of amyloid-β from the brains of mice expressing the human APOE ε4 allele. *PLoS One*. 2012;7:e41636.
40. Sperling R, Salloway S, Brooks DJ, Tampieri D, Barakos J, Fox NC, et al. Amyloid-related imaging abnormalities in patients with Alzheimer's disease treated with bapineuzumab: a retrospective analysis. *Lancet Neurol*. 2012;11:241–249.

SUPPLEMENTAL MATERIAL

SIRT1 counters cerebral hypoperfusion injury by deacetylating eNOS

Yorito Hattori, Yoko Okamoto, Takakuni Maki, Yumi Yamamoto, Naoya Oishi, Kenichi Yamahara, Kazuyuki Nagatsuka, Ryosuke Takahashi, Raj N. Kalaria, Hidenao Fukuyama, Makoto Kinoshita, Masafumi Ihara

Corresponding author: Masafumi Ihara, MD, PhD, FACP; Department of Stroke and Cerebrovascular Diseases, National Cerebral and Cardiovascular Center; 5-7-1 Fujishiro-dai, Suita, Osaka 565-8565, Japan; Telephone, (+81)-6-68335012; FAX, (+81)-6-68355137; E-mail, ihara@ncvc.go.jp

Supplemental Methods

Generation and Establishment of a Transgenic Mouse Line That Stably Expresses Mouse SIRT1 in the Brain

To generate a genetic model that chronically overexpress silent information regulator 2 homolog 1 (SIRT1) in the mouse, we constructed a transcription unit by inserting the coding region of the mouse *Sirt1* cDNA into the mouse prion gene promoter-polyA cassette which drives pan-neural gene expression. We obtained transgenic mice by injecting the linearized transcription unit into the oocytes of C57BL/6J mice and selected a founder that transmitted the transgene in Mendelian manner. We backcrossed the founder and the offspring with wild-type C57BL/6J mice for more than ten generations and established a transgenic line that gave consistent, pan-neural expression of exogenous SIRT1 in addition to the endogenous gene products. In this study we consistently analyzed male mice heterozygous for the transgene (Sirt1-Tg) with their wild-type (non-transgenic) male littermates at the age of 5–9 months old. Sirt1-Tg mice and wild-type littermates did not show recognizable differences in physical constitution and brain morphology (data not shown). All mice were maintained in the C57BL/6J background, were housed in a room with a 12-hour light/dark cycle (lights on at 7:00 a.m.) and were given access to food and water *ad libitum*. All procedures were performed in accordance with the guidelines for animal experimentation from the ethical committee of Kyoto University, and National Cerebral and Cardiovascular Center.

Surgical Procedure of Bilateral Common Carotid Artery Stenosis (BCAS) Operation

Through a midline cervical incision, both common carotid arteries were exposed. Microcoils with an internal diameter of 0.18 mm (Samini) were applied to the bilateral common carotid arteries (Supplemental Figure I). Sham-operated mice underwent the same surgical procedure without using microcoils. Anesthesia was induced with 2% isoflurane and maintained with 1.5% isoflurane in 80% nitrous oxide and 20% oxygen. Rectal temperature was maintained between 36.5°C and 37.5°C[1].

Eight-arm Radial Maze Test

As described previously[2], after 28 days post-operation, the eight-arm radial maze test was performed to examine whether spatial working memory was impaired. Each arm (8×35 cm) radiated from an octagonal central starting platform. Identical food wells were placed at the distal end of each arm. From one week before pretraining, mice were deprived of food until their body weight was reduced to 75–85% of the initial level. As the initial pretraining after deprivation of food, each mouse was placed in the central platform and allowed to explore and to consume food pellets scattered on the whole maze for a 5-min period (one session per mouse). Subsequently, these mice received another pretraining to take a pellet from each food

well after being placed at the distal end of each arm. This was repeated 8 times, using 8 different arms, for each mouse.

After these pretraining trials, actual maze acquisition trials were performed. All eight arms were baited with food pellets. Mice were placed on the central platform and allowed to get all eight pellets within 25 min. A trial was terminated immediately after all 8 pellets were consumed or 25 min had elapsed. For each trial, the number of revisiting error was recorded.

Histological Evaluation of Sirt1-Tg Mice and BCAS-operated Mice

To examine where SIRT1 was expressed in the brain, 6-μm-thick paraffin-embedded coronal sections were subjected to immunohistochemistry for silent information regulator 2 (Sir2; 1:50; Sigma-Aldrich), and cryosections (20-μm thick) were subjected to immunofluorescence for Sir2 (1:100; Sigma-Aldrich) and double immunofluorescence for Sir2 and CD31 (vascular endothelial cell, 1:500; BD Biosciences).

The brains of Sirt1-Tg mice and their littermates were dissected out at 28 days after sham or BCAS operation. Six-μm thick paraffin-embedded coronal sections were subjected to Klüver-Barrera staining. The severity of the white matter lesions was graded as normal (Grade 0), disarrangement of the nerve fibers (Grade 1), the formation of marked vacuoles (Grade 2), and the disappearance of myelinated fibers (Grade 3) in the corpus callosum. For immunohistochemistry, we used, as first antibodies, a rabbit antiglial fibrillary acidic protein antibody (a marker of astrocyte, 1:2000; DAKO), a rabbit anti-Iba1 antibody (a marker of microglia, 1:200; Wako), and a rabbit antiglutathione S-transferase-pi antibody (a marker of oligodendrocyte, 1:100; Millipore). We counted the numerical density of the glial cell nuclei with immunopositive perikarya (/0.125 mm^2) in the white matter.

Transmission Electron Microscopy

Wild-type and Sirt1-Tg mice at 2 h after sham or BCAS operation were examined by transmission electron microscopy. After mice were perfused transcardially with 0.9% saline followed by 4% paraformaldehyde and 2% glutaraldehyde in 0.1 mol/L phosphate buffer, brains were removed and consecutively sectioned at the bregma level at a thickness of 1 mm using a brain tissue matrix. Then, brain tissues were fixed by immersion in 4% paraformaldehyde and 2% glutaraldehyde in 0.1 mol/L phosphate buffer for 48 h at 4°C, and washed in 0.1 mol/L phosphate buffer (5×10 min). Two pieces of brain tissues (approximately 1.5 mm^3) were subsequently resected and postfixed with 1% osmium tetroxide for 2 h. Thereafter, the fixed tissue samples were dehydrated, infiltrated, and embedded in epoxy-resin (Luveak 812; Nakalai Tesque) for transmission electron microscope study. Ultrathin sections (80 nm) of selected areas were prepared on an ultramicrotome (EM UC6; Leica) and collected on 200-mesh cooper grids. These sections were counterstained with 2% uranyl acetate and lead citrate solution. The vessels were examined throughout the

sample with a transmission electron microscopy (H-7650; Hitachi).

Measurement of Cerebral Blood Flow (CBF)

Relative CBF was recorded by laser speckle flowmetry (Omegazone; Omegawave) which obtains high-resolution, two-dimensional imaging and has a linear relationship with absolute CBF values[3]. In the day prior to the first CBF measurement, anesthesia was induced with 2% isoflurane and maintained with 1.5% isoflurane in 80% nitrous oxide and 20% oxygen, and the scalp was removed by a midline incision so that the skull was exposed throughout the experiment. During the measurement of CBF, the skull surface was illuminated by 780 nm of laser light. The scattered light was filtered and detected by a CCD camera positioned over the head. The filter detected only scattered light that had a perpendicular polarization to the incident laser light. The raw speckle images were used to compute speckle contrast, which corresponds to the measured velocity of moving red blood cells, approximating CBF. Signal processing was performed by the algorithm developed by Forrester et al.[4]. Color-coded blood flow images were obtained in high-resolution mode (639 × 480 pixels; 1 image/sec) and the sample frequency was 60 Hz. One blood flow image was generated by averaging numbers obtained from 20 consecutive raw speckle images. The recordings were initiated after the examiner confirmed that CBF did not change over 1 min, and the five recordings of blood flow image were averaged. In order to prevent the fluctuation of CBF and blood pressure during the measurement of CBF, anesthesia was induced as stated above. During the measurement of CBF, mice were held in a small plastic holder on a warming pad and thermostatically controlled at 36.5°C to 37.5°C in rectal temperature. Blood pressure was measured by the tail cuff method and confirmed to be kept constant.

Evaluation of Vascular Response to Acetylcholine (ACh) and S-Nitroso-N-acetyl-DL-penicillamine (SNAP)

To evaluate vascular responses to vasodilatory stimuli, a cranial window preparation was performed as previously reported with modification[5, 6]. In brief, a 3 mm × 3 mm diameter craniotomy was performed with dental drill in the right parietal bone and the dura mater was removed. The endothelium-dependent vasodilator ACh (100 μmol/L; Sigma-Aldrich), endothelial nitric oxide synthase (eNOS)-agonist, or S-Nitroso-N-acetyl-DL-penicillamine (SNAP; 500 μmol/L; Sigma-Aldrich), nitric oxide donor, were infused into the cranial window at a rate of 100 μL/min for 5 min. The CBF and the vasodilative changes in response to ACh or SNAP were evaluated at 5 min after infusion. CBF increase during the 5 min after infusing was taken as response amplitude using laser speckle flowmetry. The rate of CBF increase after infusing was calculated as the CBF increase (%) divided by the baseline CBF. Next, we assessed the vasodilatative responses. For real-time *in vivo* imaging of the cerebral vessels, we used fibered fluorescence microscopy (MVX10; Olympus). After intravenous tail

vein injection of fluorescein isothiocyanate-dextran (2×10^6 molecular weight, 200 μL of 20 mg/mL; Sigma-Aldrich), the leptomeningeal vessels were visualized. Averaged vessel diameters across a 25 μm longitudinal segment (5 consecutive segments per mouse) of the dorsal middle cerebral arteries were analyzed as previously described[5]. Peak vessel diameter increase during the 5 min was taken as response amplitude. Data were calculated as %vasodilation vs. baseline vessel diameter. We distinguished penetrating arteries from bridging (collecting) veins by identifying the location and also by following the direction of flow from the pial surface.

Western Blot Analysis

The brains of BCAS-operated mice were dissected out before and at 2 h after BCAS and cut coronally into 5-mm thick slices (bregma -3 to +2 mm) and homogenized in radioimmunoprecipitation assay buffer containing a protease and phosphatase inhibitor mixture (Nakarai Tesque). The amount of proteins applied to each well was 80 μg for acetylated eNOS, non-acetylated eNOS, 40 μg for eNOS and phosphorylated eNOS, and 20 μg for β-actin. Samples were electrophoresed on SDS-polyacrylamide minigels and the proteins were transferred to polyvinylidene difluoride membranes (Bio-Rad). Membranes were incubated with primary antibodies against eNOS (1:2500; BD Biosciences), phospho-eNOS (Ser1177) (1:1000; Cell Signaling Technology) and β-actin (1:5000; Sigma-Aldrich). The signal was visualized using horseradish peroxidase-conjugated secondary antibodies with Luminata Forte Western HRP substrate (Millipore). Immunoblot membranes were developed using the LAS-4000 Imaging System (Fujifilim). The densitometric measurement of immunoblots was performed using Image-J (NIH).

Similarly, brain homogenates of cerebral cortex, caudoputamen, midbrain, brainstem, cerebellum, and spinal cord were immunoblotted using anti-Sir2 antibody (1:500; Sigma-Aldrich) and anti-GAPDH antibody (1:1000; Cell Signaling Technology).

Analysis of eNOS Acetylation/Non-acetylation

To determine acetylation or non-acetylation status of eNOS, brain homogenates before and at 2 h after BCAS were first immunoprecipitated by anti-acetylated-lysine antibody (1:100; Cell Signaling Technology) using Immunoprecipitation Kit-Dynabeads Protein A (Life technologies). As a result, the brain homogenates were separated into bound and unbound fractions to the anti-acetylated-lysine antibodies. The bound fraction was eluted with elution buffer as a fraction that contains total acetylated proteins. The both fractions were then immnunoblotted with eNOS to detect acetylated and non-acetylated eNOS, respectively, using the immunoblotting method as stated above.

Exogenous Administration of Sirtinol

To examine whether sirtinol (Sigma-Aldrich), SIRT1 inhibitor, abolished CBF-preserving effect of SIRT1, sirtinol was intravenously injected into 10-week-old Sirt1-Tg mice with the dose of 1 mg/kg (dimethyl sulfoxide 50 μL + saline 100 μL) immediately before sham or BCAS operation. The CBF estimate was carried out using laser speckle flowmetry as described above. CBF was expressed as a percentage of baseline flow.

Exogenous Administration of Cavtratin

Caveolin-1 scaffolding domain peptide (ENZO Life Sciences), eNOS inhibitor called cavtratin, was intraperitoneally injected into 10-week-old Sirt1-Tg mice with the dose of 10 mg/kg/day (dimethyl sulfoxide 60 μL + saline 90 μL) for 3 consecutive days prior to sham or BCAS operation. Last injection was carried out at 24 h prior to each surgery. The CBF estimate was carried out using laser speckle flowmetry as described above. CBF was expressed as a percentage of baseline flow.

Visualization of Cerebral Angioarchitecture

The cerebral angioarchitecture was studied by the postmortem latex perfusion technique. The root of the ascending aorta was cannulated with flexible plastic tubing (0.65 mm external diameter). The tubing was connected to a 5 mL syringe, the cannulated aorta, and a mercury manometer, establishing a closed circuit to monitor perfusion pressure. Immediately after 2 mL saline injection, 4mL white latex compound (Chicago Latex Products) mixed with 50 μL/mL carbon black (Bokusai) diluted 2:1 with saline was injected at a perfusion pressure of 150 mmHg over a 5-min period. After the initiation of infusion, the right atrium of the heart was incised to allow for venous outflow. In order to harden the latex completely for the brain removal procedure, the dead animal was soaked in ice-cold water 20 min after the end of infusion, and the brain was subsequently removed 20 min later. Photographs of dorsal and ventral surface of the brain were taken using a digital microscope (DinoLite; AnMo Electronics Corp.) at ×80 magnification. The vessel diameter of the circle of Willis was measured using image analysis software (DinoCapture; AnMo Electronics Corp.). The diameters of the internal carotid artery, the anterior cerebral artery, the middle cerebral artery and the posterior communicating artery were averaged across both sides. The diameters of the internal carotid artery and middle cerebral artery were measured just proximally and distally to the terminal bifurcation of the internal carotid artery, respectively. The diameter of the anterior cerebral artery was measured just proximally to the origin of the olfactory artery. The diameter of the posterior communicating artery was measured at its origin from the internal carotid artery.

Statistical Analysis

Statistical analysis was conducted using StatView (SAS Institute). All values are expressed as

means ± standard error of the mean in the figures. Data were analyzed by unpaired t-test unless noted otherwise. Differences with $p<0.05$ were considered statistically significant in all analyses.

Supplemental References

1. Shibata M, Ohtani R, Ihara M, Tomimoto H. White matter lesions and glial activation in a novel mouse model of chronic cerebral hypoperfusion. *Stroke*. 2004;35:2598-2603.
2. Shibata M, Yamasaki N, Miyakawa T, Kalaria RN, Fujita Y, Ohtani R, et al. Selective impairment of working memory in a mouse model of chronic cerebral hypoperfusion. *Stroke*. 2007;38:2826-2832.
3. Ayata C, Dunn AK, Gursoy OY, Huang Z, Boas DA, Moskowitz MA. Laser speckle flowmetry for the study of cerebrovascular physiology in normal and ischemic mouse cortex. *J Cereb Blood Flow Metab*. 2004;24:744-755.
4. Forrester KR, Stewart C, Tulip J, Leonard C, Bray RC. Comparison of laser speckle and laser doppler perfusion imaging: Measurement in human skin and rabbit articular tissue. *Med Biol Eng Comput*. 2002;40:687-697.
5. Han BH, Zhou ML, Abousaleh F, Brendza RP, Dietrich HH, Koenigsknecht-Talboo J, et al. Cerebrovascular dysfunction in amyloid precursor protein transgenic mice: Contribution of soluble and insoluble amyloid-beta peptide, partial restoration via gamma-secretase inhibition. *J Neurosci*. 2008;28:13542-13550.
6. Park L, Wang G, Zhou P, Zhou J, Pitstick R, Previti ML, et al. Scavenger receptor CD36 is essential for the cerebrovascular oxidative stress and neurovascular dysfunction induced by amyloid-beta. *Proc Natl Acad Sci U S A*. 2011;108:5063-5068.

Supplemental Figure I

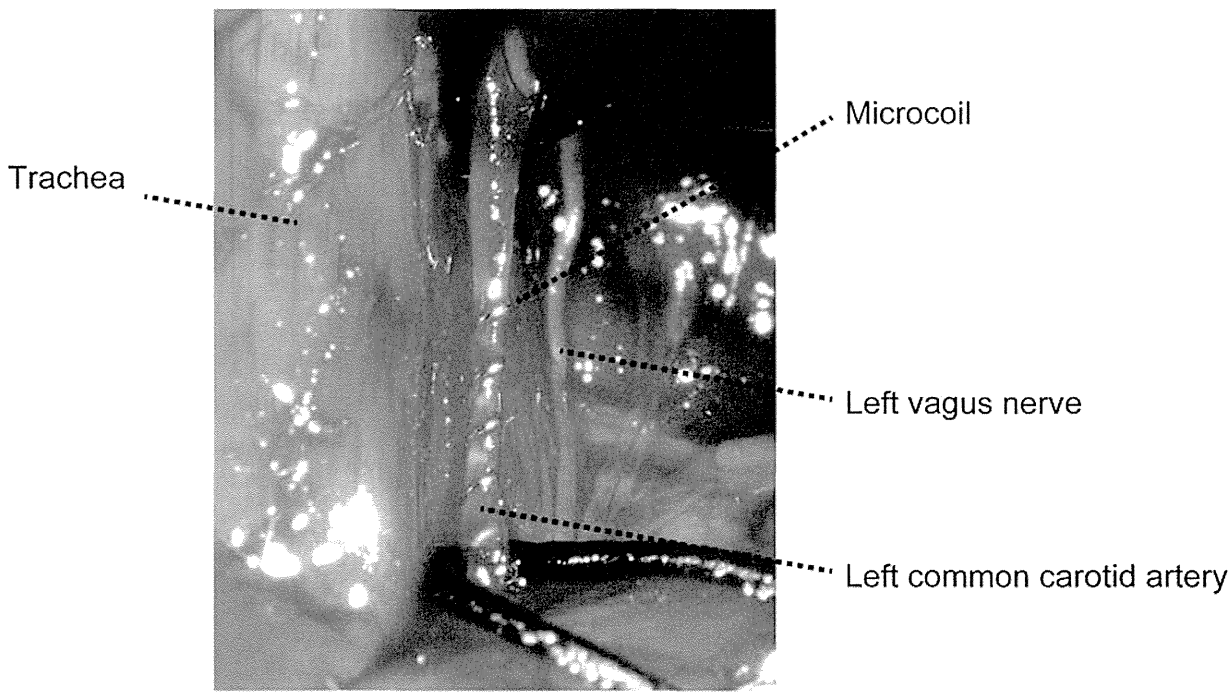

Supplemental Figure I: Representative image showing surgical implantation of a microcoil on the common carotid artery

A microcoil is placed on the left common carotid artery after the vagus nerve is separated from the carotid artery.

Supplemental Figure II

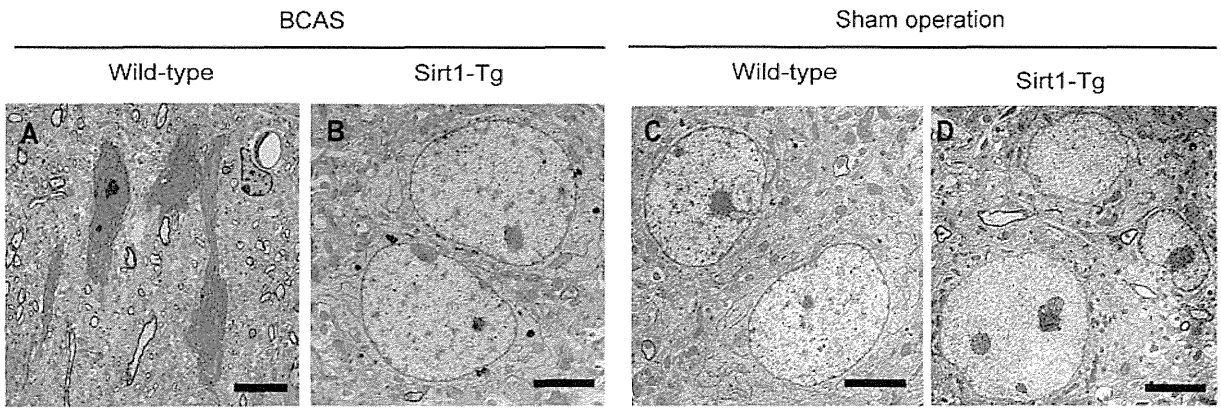

Supplemental Figure II: SIRT1 rescued neuronal injuries after BCAS
Transmission electron microscopic images of BCAS-operated, wild-type (A) or Sirt1-Tg mice (B), and sham-operated, wild-type (C) or Sirt1-Tg mice (D) at 2 h after each surgery. (A) Neurons of a wild-type mouse undergo shrinkage of nuclei and cytoplasm. (B–D) Neurons appear normal. Scale bars indicate 10 μm (A), and 20 μm (B–D).

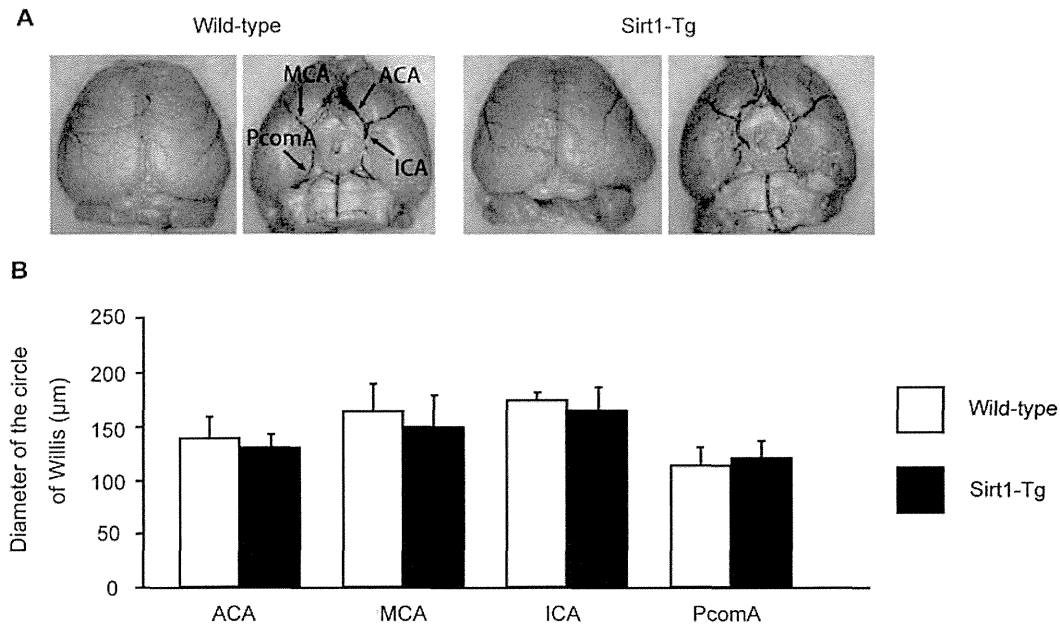

Supplemental Figure III: Similar angioarchitecture of wild-type littermates and Sirt1-Tg mice

(A) Representative images of the dorsal and ventral cerebral angioarchitecture by postmortem latex perfusion method of the wild-type and Sirt1-Tg mouse. Abbreviations: ACA, anterior cerebral artery; MCA, middle cerebral artery; ICA, internal carotid artery; PcomA, posterior communicating artery. (B) Histograms showing the mean diameters of ACA, MCA, ICA and PcomA of wild-type (n = 6) and Sirt1-Tg mice (n = 5).

Supplemental Figure IV

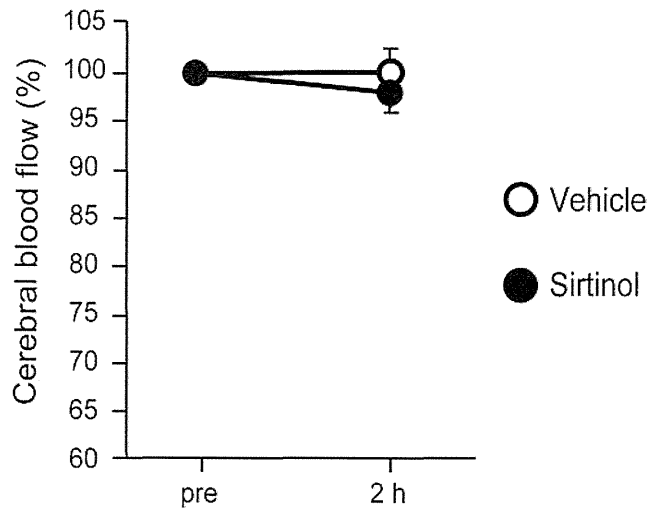

Supplemental Figure IV: Sham operation did not alter CBF of sirtinol-treated Sirt1-Tg mice.

Temporal profiles of CBF of vehicle-treated Sirt1-Tg mice (n = 3) and sirtinol-treated Sirt1-Tg mice (n = 3) before and at 2 h after sham operation.

Supplemental Figure V

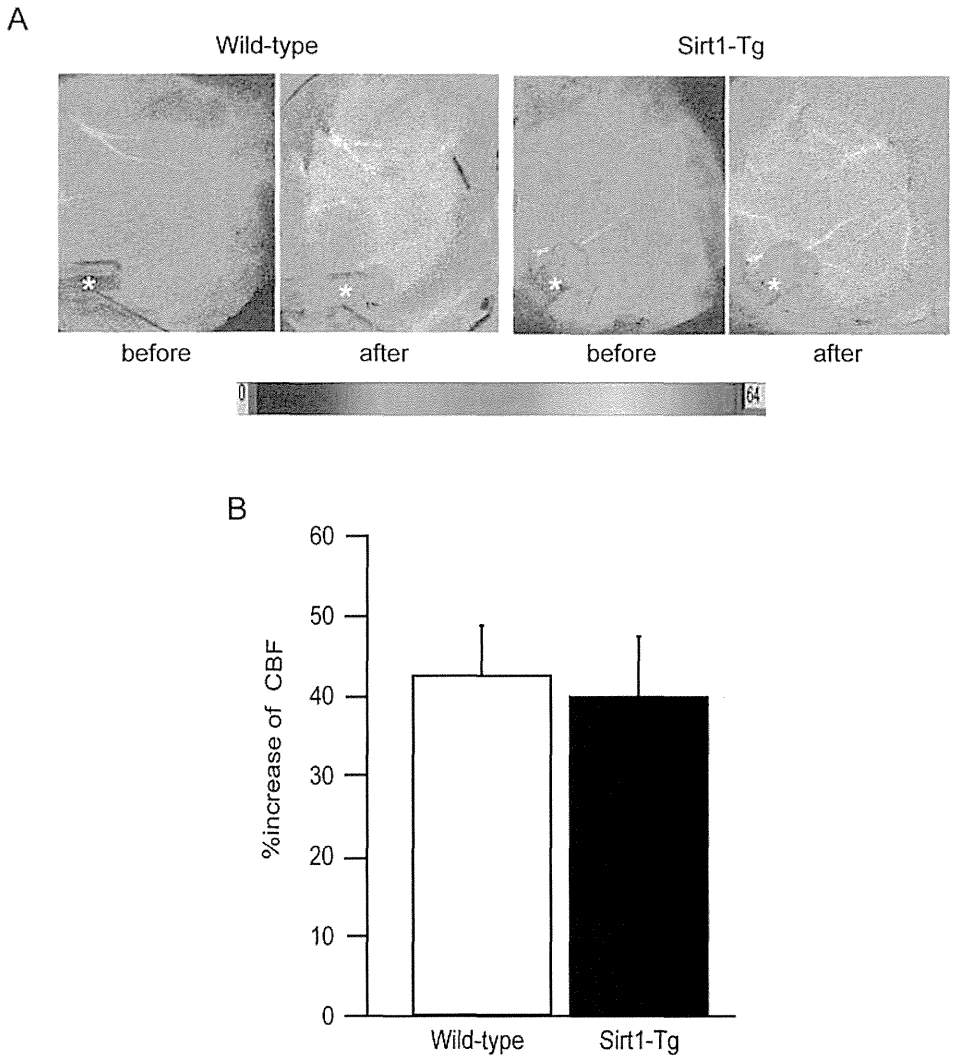

Supplemental Figure V: Temporal changes in CBF before and after perfusion of SNAP on brain surface in wild-type (n = 3) and Sirt1-Tg mice (n = 3)
(A) Representative CBF images assessed by laser speckle flowmetry before (left) and after (right) perfusion of SNAP. * indicates an inlet of SNAP. (B) Histogram showing %increase of CBF assessed by laser speckle flowmetry.

Supplemental Figure VI

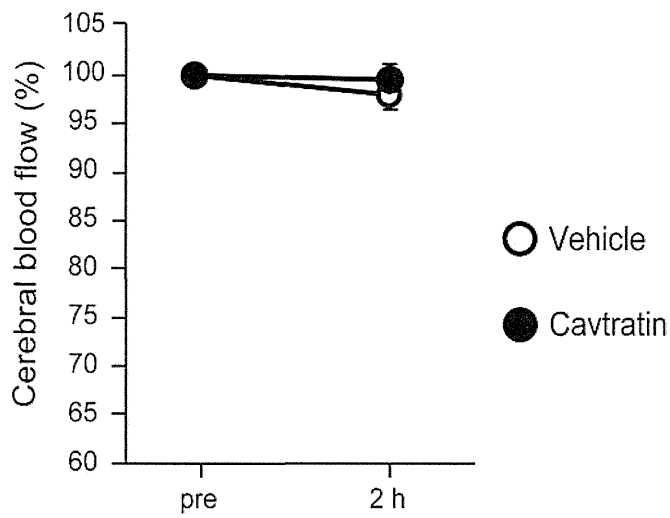

Supplemental Figure VI: Sham operation did not alter CBF of cavtratin-treated Sirt1-Tg mice.

Temporal profiles of CBF of vehicle-treated Sirt1-Tg mice (n = 3) and cavtratin-treated Sirt1-Tg mice (n = 3) before and at 2 h after sham operation.

Stroke
JOURNAL OF THE AMERICAN HEART ASSOCIATION

Silent Information Regulator 2 Homolog 1 Counters Cerebral Hypoperfusion Injury by Deacetylating Endothelial Nitric Oxide Synthase

Yorito Hattori, Yoko Okamoto, Takakuni Maki, Yumi Yamamoto, Naoya Oishi, Kenichi Yamahara, Kazuyuki Nagatsuka, Ryosuke Takahashi, Raj N. Kalaria, Hidenao Fukuyama, Makoto Kinoshita and Masafumi Ihara

Stroke. 2014;45:3403-3411; originally published online September 11, 2014;
doi: 10.1161/STROKEAHA.114.006265
Stroke is published by the American Heart Association, 7272 Greenville Avenue, Dallas, TX 75231

Print ISSN: 0039-2499. Online ISSN: 1524-4628

ANNALS of Clinical and Translational Neurology
Open Access
AMERICAN NEUROLOGICAL ASSOCIATION

RESEARCH ARTICLE

Phosphodiesterase III inhibitor promotes drainage of cerebrovascular β-amyloid

Takakuni Maki[1,2], Yoko Okamoto[1,3], Roxana O. Carare[4], Yoshiki Hase[1], Yorito Hattori[1,5], Cheryl A. Hawkes[4], Satoshi Saito[1,5], Yumi Yamamoto[5], Yasukazu Terasaki[2], Hatsue Ishibashi-Ueda[3], Akihiko Taguchi[6], Ryosuke Takahashi[1], Taihei Miyakawa[7], Raj N. Kalaria[8], Eng H. Lo[2], Ken Arai[2] & Masafumi Ihara[1,9]

[1]Department of Neurology, Graduate School of Medicine, Kyoto University, Kyoto, Japan
[2]Departments of Radiology and Neurology, Massachusetts General Hospital and Harvard Medical School, Charlestown, Massachusetts
[3]Department of Pathology, National Cerebral and Cardiovascular Center, Osaka, Japan
[4]Division of Clinical Neurosciences, Southampton General Hospital, Southampton University, Hampshire, United Kingdom
[5]Department of Regenerative Medicine and Tissue Engineering, National Cerebral and Cardiovascular Center, Osaka, Japan
[6]Department of Regenerative Medicine Research, Institute of Biomedical Research and Innovation, Kobe, Japan
[7]Amakusa Hospital, Kumamoto, Japan
[8]Institute for Ageing and Health, NIHR Biomedical Research Building, Newcastle University, Campus for Ageing and Vitality, Newcastle upon Tyne, United Kingdom
[9]Department of Stroke and Cerebrovascular Diseases, National Cerebral and Cardiovascular Center, Osaka, Japan

Correspondence
Masafumi Ihara, Department of Stroke and Cerebrovascular Diseases, National Cerebral and Cardiovascular Center, 5-7-1 Fujishiro-dai, Suita, Osaka 565-8565, Japan. Tel: +81-6-6833-5012; Fax: +81-6-6835-5137; E-mail:ihara@ncvc.go.jp
Takakuni Maki, Departments of Radiology and Neurology, Massachusetts General Hospital and Harvard Medical School, MGH East 149-2401, Charlestown, MA 02129. Tel: +1-617-724-9503; Fax: +1-612-726-7830; E-mail: tmaki@partners.org

Funding Information
We gratefully acknowledge grant support from the Ministry of Health, Labour and Welfare (M. I., No. 0605-1), the Ministry of Education, Culture, Sports, Science and Technology (M. I., Scientific Research (B), No. 23390233), the Takeda Science Foundation (M. I.), the National Institutes of Health (K. A., E. H. L., P01 NS055104; K. A., R01 NS065089; E. H. L., R37 NS037074), the Research Councils UK and Alzheimer's Research UK (R. N. K.), the Japan Society for the Promotion of Science (T. M.), and the Uehara Memorial Foundation (T. M.).

Received: 17 December 2013; Revised: 9 April 2014; Accepted: 2 June 2014

Abstract

Objective: Brain amyloidosis is a key feature of Alzheimer's disease (AD). It also incorporates cerebrovascular amyloid β (Aβ) in the form of cerebral amyloid angiopathy (CAA) involving neurovascular dysfunction. We have recently shown by retrospective analysis that patients with mild cognitive impairment receiving a vasoactive drug cilostazol, a selective inhibitor of phosphodiesterase (PDE) III, exhibit significantly reduced cognitive decline. Here, we tested whether cilostazol protects against the disruption of the neurovascular unit and facilitates the arterial pulsation-driven perivascular drainage of Aβ in AD/CAA. **Methods:** We explored the expression of PDE III in postmortem human brain tissue followed by a series of experiments examining the effects of cilostazol on Aβ metabolism in transgenic mice (Tg-SwDI mice) as a model of cerebrovascular β-amyloidosis, as well as cultured neurons. **Results:** We established that PDE III is abnormally upregulated in cerebral blood vessels of AD and CAA subjects and closely correlates with vascular amyloid burden. Furthermore, we demonstrated that cilostazol treatment maintained cerebral hyperemic and vasodilative responses to hypercapnia and acetylcholine, suppressed degeneration of pericytes and vascular smooth muscle cells, promoted perivascular drainage of soluble fluorescent $A\beta_{1\text{-}40}$, and rescued cognitive deficits in Tg-SwDI mice. Although cilostazol decreased endogenous Aβ production in cultured neurons, C-terminal fragment of amyloid precursor protein expression was not altered in cilostazol-treated Tg-SwDI mice. **Interpretation:** The predominant action of cilostazol on Aβ metabolism is likely to facilitate Aβ clearance due to the sustained cerebrovascular function in vivo. Our findings mechanistically demonstrate that cilostazol is a promising therapeutic approach for AD and CAA.

doi: 10.1002/acn3.79